Evolution of Orogenic Plateaus at Subduction Zones

Fernandez-Blanco, D.

2014

document version
Publisher's PDF, also known as Version of record

3

Central Domain of the Central Anatolian Plateau*

Contents

*Based on published article: D. Fernández-Blanco, G. Bertotti and A. Çiner (2013), Cenozoic Tectonics of the Tuz Gölü Basin (Central Anatolia Plateau, Turkey), *Turkish Journal of Earth Sciences*, doi: 10.3906/yer-1206-7

"The greatness of a man is not in how much wealth he acquires,
but in his integrity and his ability to affect
those around him positively."

Bob Marley

Abstract

We present a new 3D geologic model for the architecture and Cenozoic tectonic evolution of the Tuz Gölü Basin, a major sedimentary basin in the Central Anatolian orogenic plateau. This model is grounded on seven depth-converted seismic reflection profiles, in combination with the analysis of backstripped subsidence curves, isochore maps, and a palinspastically restored cross-section. Two stages of basin formation are detected during Cenozoic times. During the Palæogene, around 2 km *of basement subsidence led to the development of a sag basin broader than the present basin in the absence of bounding faults. After a period of uplift and erosion, sedimentation restarted by Tortonian times. Up to* 3.5 km *of post−Palæogene sediments were deposited in relation to this second regional subsidence phase, which continued possibly well into the Pliocene. During this time, the two main fault systems found in the area, the Tuz Gölü and the Sultanhanı faults, developed as south-west dipping, NW−SE striking, normal faults. At some time in the Late Miocene−Early Pliocene, during regional subsidence, a previously unreported phase of contraction occurred, which led to the development of a north-east−vergent thrust sheet, the culmination of which forms the morphologic ridge to the east of the Tuz Gölü Lake. This structure presently divides the previously continuous Tuz Gölü Basin. Finally, minor extensional reactivation occurred. At the regional scale, the pre−Late Miocene subsidence is coeval with the initiation of volcanism in the Central Anatolian Volcanic Province and marine carbonate deposition in southern Turkey, and the latest Miocene shortening is (partly) contemporaneous with the onset of uplift in the same region.*

3.1 Introduction

Collision between Eurasian and Arabian plates initiated orogenic build-up and crustal shortening in the Eastern Anatolia Plateau [e.g. Şengör and Yılmaz, 1981; Dewey et al., 1986; Keskin, 2003; Okay et al., 2010]. To the west, the Neogene Central Anatolian Plateau (CAP), delineated by the Pontide and Tauride mountain ranges, has a less clear kinematic and geodynamic evolution due to the scarcity of structural data on the Miocene rocks.

Prior to CAP formation, during Late Cretaceous to Late Palæocene, several continental blocks collided in Turkey [e.g. Şengör and Yılmaz, 1981; Dewey et al., 1986; Görür et al., 1984, 1998; Williams et al., 1995; Robertson, 1998b; Hüsing et al., 2009]. This continental gathering caused regional uplift that led to fluvio-lacustrine deposition in the central domains [e.g. Görür et al., 1984], and initial formation of topography and rise above to sea-level in both the Pontides and the Taurides. This happened by Eocene times in the Pontides [e.g. Şengör and Yılmaz, 1981; Şengör et al., 1984], as shown by non-marine deposition and the absence of Upper Palæogene rocks [e.g. Robinson et al., 1995; Rojay, 1995], and by the Early Oligocene in the Taurides [e.g. Jaffey and Robertson, 2005; Eriş et al., 2005], where continental deposition took place [e.g. Bassant et al., 2005; Şafak et al., 2005].

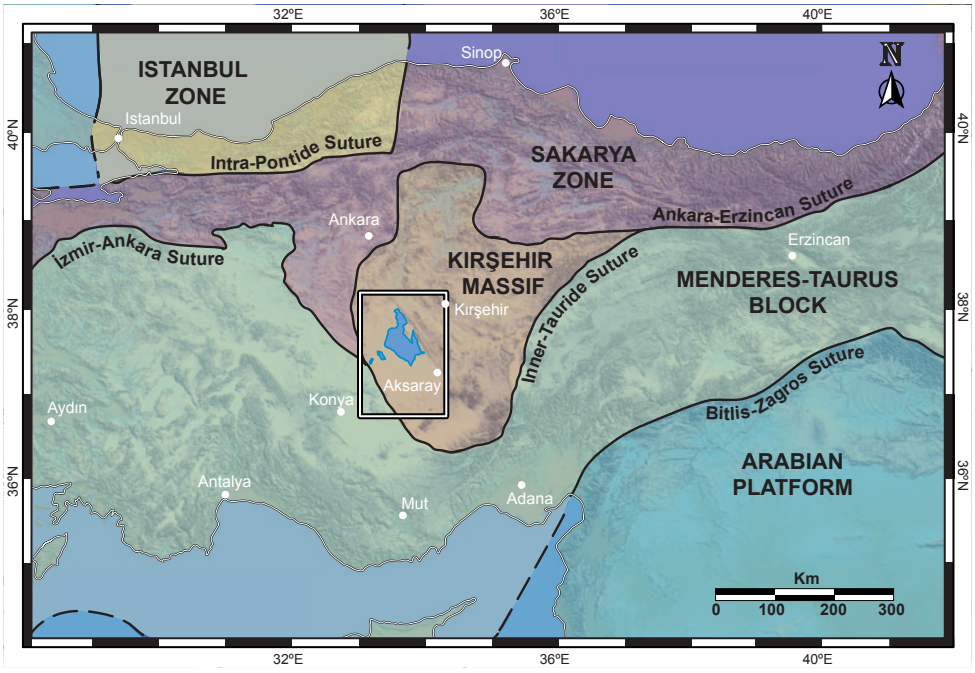

Figure 3.1: *Palæoterrains map of the area, showing the main tectonic elements of Turkey and the location of the study area. Slight modification on the location of the boundaries after [Okay and Tüysüz, 1999] is based on analysis of* 1 arc *DEM and LandSat 7 images set from the NASA.*

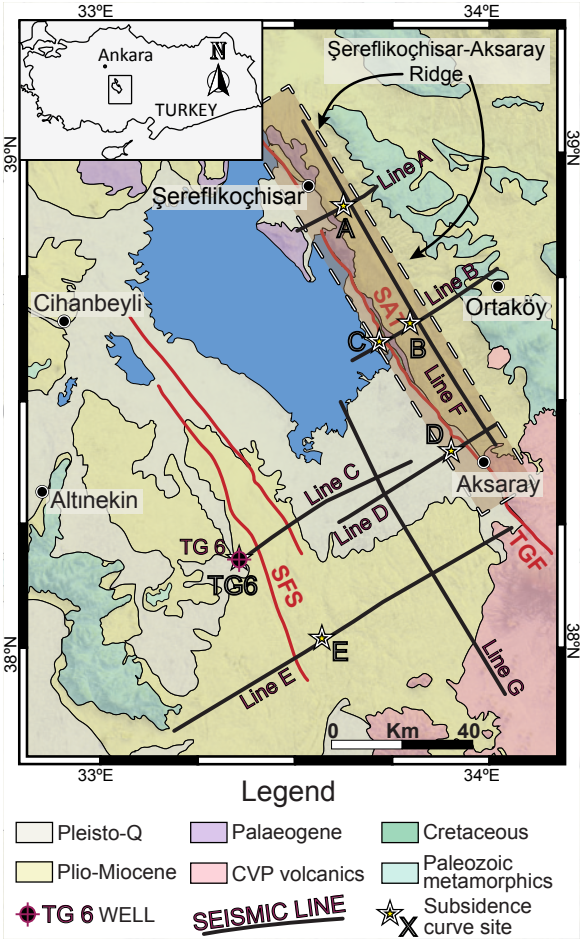

Figure 3.2: *Tuz Gölü Basin geologic and data location map, depicting lithological distribution as in the MTA geologic map. Location of the seven interpreted seismic reflection lines and the TG6 borehole is shown as well as the position of the sites chosen for subsidence analysis. The main fault systems are illustrated in red.*

Subsequently, a period of regional subsidence developed, which initiated deposition of marine sediments in the south and north of the plateau. Meanwhile, in Central Anatolia the continued deposition of continental sediments led to formation of a system of Late Cenozoic or younger interior basins [Çemen et al., 1999]. The end of marine sedimentation in the southern margin of the CAP [Bassant et al., 2005; Çiner et al., 2008], probably marking the onset of the succeeding surface uplift event, has been recently dated by Cosentino et al. [2012] to be as young as ∼8 Ma. Similarly, the surface uplift in the northern margin of the plateau has been reported to be Late Miocene-Early Pliocene [Yıldırım et al., 2011]. However, these uplift events have not been linked with the center of the system and the tectonic regime in the CAP interior during Miocene times is still under debate [see Genç and Yürür, 2010, for a recent example]. Understanding the structural pattern as well as the accurate timing of main deformation events in the area will give relevant constraints on the mode and genetic nature of the CAP build-up and information on plateau genesis elsewhere.

Previous studies in the Central Anatolia are centered on its pre-Miocene evolution [e.g. Uğurtaş, 1975; Şengör and Yılmaz, 1981; Görür et al., 1984]. Early works were mostly concentrated on sedimentological approaches [e.g. Arıkan, 1975], whereas more recent studies used geophysical data [Gürbüz and Evans, 1991; Aydemir and Ateş, 2005, 2006b, a, 2008; Onal et al., 2008]. On the other hand, several studies centered on the present tectonic regime and type of faulting [Dirik and Göncüoğlu, 1996; Çemen et al., 1999; Özsayın and Dirik, 2007, 2011].

The Tuz Gölü Basin (TGB) is a major representative amongst the CAP interior basins [Dirik and Erol, 2000]. Here, we aim to reconstruct the Miocene structural evolution of the TGB and surrounding areas in relation to its regional context. For this, we have interpreted and converted to depth seven seismic reflection profiles at eastern and southern locations with respect to the Tuz Gölü lake, analyzing structures and sedimentary body geometries. On the basis of the of the geological sections we have constructed the following for the Miocene units; *(i)* isochore maps to resolve their sedimentary distribution, *(ii)* backstripped subsidence curves to determine the vertical movements, and *(iii)* a palinspastically retrodeformed section, to quantify the horizontal deformations. The horizontal motions have been then compared with the vertical motions. The final output is a 3D evolutionary model for the tectonic movements undergone by the area since Palæogene times.

3.2 Study area

The study area is located in central Turkey, at an averaged elevation of about 1.1 km, covering a relevant part of the Tuz Gölü Basin (s.l.) (as defined by Görür et al. [1984]). A NW−SE trending relief called Şereflikoçhisar−Aksaray Ridge (SAR) stands out of the remarkably flat topography of the Tuz Gölü Lake and its surroundings (Fig. 3.2). Presently, the central domain of the study area is mostly covered by unconformable Miocene or younger units, with the exception of an elongated area of Cretaceous and Palæogene rocks that outcrop along the SAR (Fig. 3.2). The SAR is bounded to the south-west by the Tuz Gölü Fault (TGF). Oriented parallel to the elongation of the high relief, the south-west dipping TGF represents one of the most important structures in Central Anatolia. This dextrally oblique normal fault [Dirik and Erol, 2000; Huvaz, 2009], together with the strike-slip Yeniceoba−Cihanbeyli Fault System in the west [Özsayın and Dirik, 2007] and its southward continuation, the Sultanhanı Fault System (SFS), have being classically considered to be basin-forming structures (see Fig. 3.2).

3.3 Data and methods

The TG6 well and seven seismic reflection profiles were selected for interpretation from the data set provided by the General Directorate of Petroleum Affairs (data set obtained by Turkish Petroleum Corporation (TPAO) in the 1990 and 1991 campaigns). The lines are located around the present-day Tuz Gölü Lake; five of them are perpendicular to the SAR, two parallel to it (Fig. 3.2). The NE−SW seismic lines transverse the main structures of the basin whereas the two parallel profiles image the basin extent in the NNW−SSE direction. The raw seismic images of the lines can be seen in Appendix A.

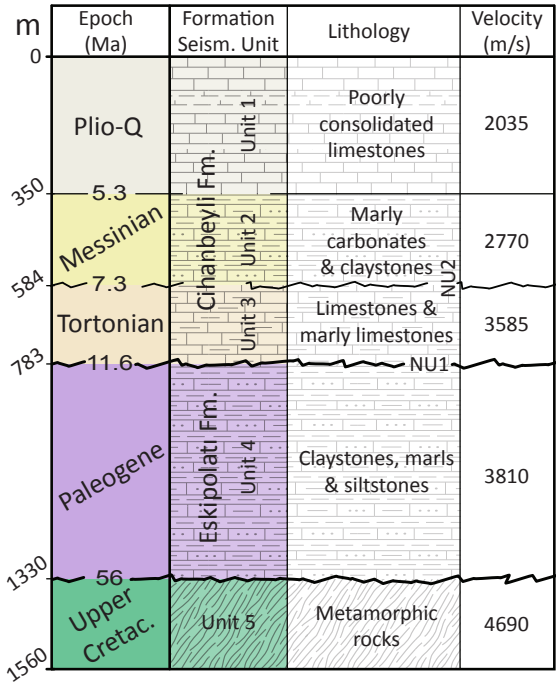

Figure 3.3: *TG6 well data and velocity model adopted for depth conversion. Within the Miocene package, different intervals are defined on the base of strong lithological contrasts in conjunction with changes in the sonic log signal. Mean average interval velocities are obtained assuming constant velocities along each unit interval, and defined taking into account the slowness signal and the different fractions of lithology content of each unit.*

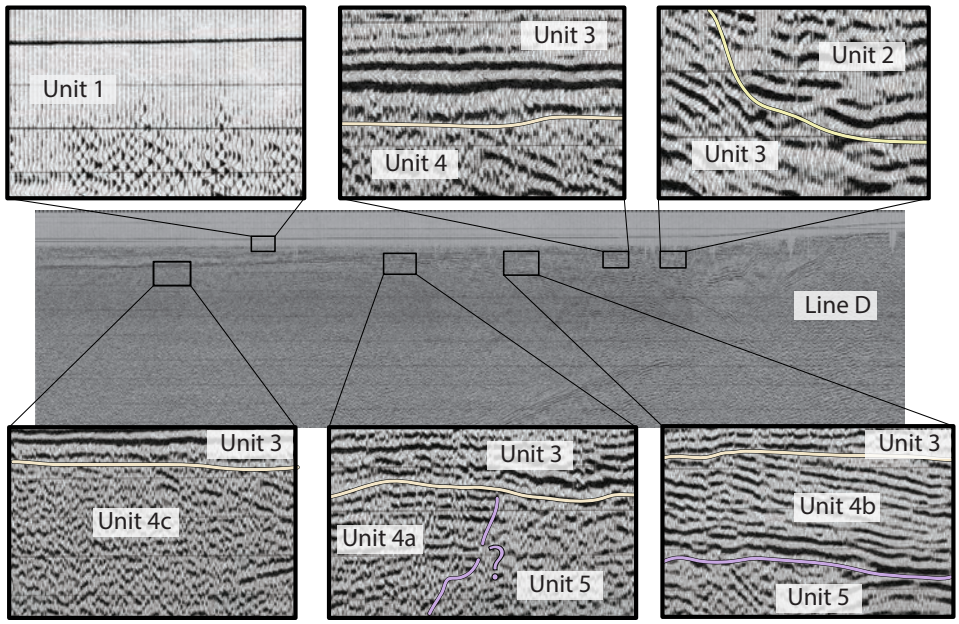

Figure 3.4: *Main seismic facies identified for the seismic sections of the study area, shown in line D.*

The lines cover some 120 km in the north-east direction and ca. 170 km in the NNW direction, with a lateral separation between them of around 30 km in both directions (Fig. 3.2). The seismic lines were originally supplied as .tiff images and were then converted to SegY format using GeoSuite AllWorks® and the original recording parameters. Analysis of the seismic signal and interpretation were made on the time section and then converted to depth on the base of sonic log velocities from the well TG6 (Fig. 3.3).

3.3.1 Seismic facies and units

The Unit 1, in the uppermost part of the seismic images, has none or very weak reflections, being mostly transparent due to lack of signal in at least the first $200 - 400$ ms. Its base was chosen by means of lithological and seismic velocity characteristics observed in the TG6 well and extended along the rest of the lines Fig. 3.4.

Unit 2 is a seismic package of continuous and rhythmic but often weak reflections. A low angle erosional unconformity marks the base boundary of the Unit 2. This surface is a clear diagnostic feature of the seismic lines (Fig. 3.4) and corresponds to the Neogene Unconformity 2 (NU2) of Uğurtaş [1975]. The NU2 cannot be correlated throughout the study area as it becomes less angular in many locations.

Below the NU2, Unit 3 is a characteristic seismic package with continuous and generally high-frequency rhythmic reflections. The bottom of Unit 3 is formed by two very strong positive regional reflections followed by a low reflective area. The underlying angular unconformity marks the base of this unit. This regional surface, named Neogene Unconformity 1 (NU1) in Uğurtaş [1975] corresponds to the base of the Miocene deposits in the area. This unconformity encompasses a hiatus of up to 17 My [Genç and Yürür, 2010] (see Figs. 3.3 and 3.4).

Three different situations can be found for the distribution of units below the Miocene (Fig. 3.4); *(i)* areas where Unit 3 is unconformably above the incoherent and/or irregularly distributed low-frequency reflections of Unit 5, *(ii)* areas where Unit 3 is above a package of mid-frequency laterally discontinuous deformed reflections, named Unit 4, which is in turn unconformably deposited on top of the Unit 5, and *(iii)* areas where the unclear nature of the reflections does not permit discrimination between units 4 and 5. Unit 4 generally corresponds to Palæogene rocks. To the south-west of the study area, Unit 4 might instead correspond to evaporitic bodies, as stated in the study carried out by Uğurtaş [1975], who defined the presence of salt walls with closer-spaced, higher-definition seismic lines. Unit 5 represents the acoustic basement formed by metamorphic rocks.

3.3.2 Seismic–to–well tie and time–to–depth conversion

The seismic–to–well "tie" is a common technique used to associate geological units to the seismic units defined by seismic facies analysis, thus assigning geologic value to the seismic signal. See Chapter 2.

One single well (TG6 well) that contained a (partial) sonic log record was available for analysis (see Fig. 3.2 and Fig. 3.3). The TG6 well penetrates 1560 m of Eocene-Recent carbonates, marls, silts and sands before it reaches the rocks of the Cretaceous ophiolitic mélange [Derman et al., 2000]. The defined Quaternary to

Cenozoic formations are described as Cihanbeyli and Eskipolatlı formations for the area, and the assigned ages at their base are Tortonian and Eocene, respectively [Görür et al., 1984; Huvaz, 2012*pers. comm.*]. The Cihanbeyli Formation (upper 783 m) is formed by limestones, marls and clays (Fig. 3.3).

Three intervals were defined within the Cihanbeyli Formation on the basis of interval velocity, lithological differences and seismic facies characteristics (see Chapter 2). The basal interval is correlated with the base of the Cihanbeyli Formation, aged Tortonian [Huvaz, 2012*pers. comm.*]. The upper interval presents typical interval velocities of unconsolidated sediments and is therefore assigned to be Pliocene−Q in age. The intermediate interval shows distinctive seismic velocities, varying more than 500 m/s with respect to either the basal or the top intervals. This interval shows as well a distinctive seismic facies character. Therefore, this interval is assumed to correspond to sediments of roughly Messinian age. Thus, the basal surface of these intervals/units roughly corresponds to Pliocene (Unit 1), Messinian (Unit 2) and Tortonian (Unit 3). The Eskipolatlı Formation is enclosed between unconformities and comprises 547 m of clay, marls and silts. This Formation is Palæogene in age and it is considered to correspond to Unit 4. Unit 5 is linked with Cretaceous rocks.

After definition of these units, the TG6 well was linked to seismic line C, which passes through the well site. Since the seismic lines cross-cut each other (Fig. 3.2), these newly defined horizons were used for correlation throughout the area by means of the seismic facies. This correlation was partly direct, continuing specific seismic facies units, and partly jump-correlated, where no direct connection amongst reflections was possible. The latter procedure is followed for the base of Unit 1 and for the contact between units 4 and 5, where differentiation between both units is often not clear.

In order to avoid time-related artefacts, the seismic lines presented here were converted to true depth using the GeoSuite AllWorks® software and the velocity values shown in Fig. 3.3 (see also Chapter 2). The average interval velocities were obtained assuming constant slowness velocities in each depth interval and weighted lithological standard velocities [Bourbié et al., 1987]. Among the available techniques, this method is geologically the most reliable, considering both the non-uniqueness associated with the construction of velocity models [Al-Chalabi, 1997b, a; Reilly, 1993] and that Dix equations [Dix, 1955] are only valid for homogeneous isotropic low-steepness layers. Although using standard velocity values extracted from the sonic log is a rough approach, it is appropriate for our purposes as no important variation in density or in compaction by overburden can be assumed. Furthermore, the obtained values (Fig. 3.3) are consistent with those of Aydemir and Ateş [2006b, a].

3.4 The seismic lines

3.4.1 The NE−SW-trending seismic sections

Seismic line A

This seismic line is the northernmost section in the study area. Located near the Tuz Gölü Lake, line A partly covers the small Şereflikoçhisar peninsula, crosses the Şereflikoçhisar−Aksaray Ridge (SAR) and continues to the north-east (Fig. 3.2).

The SAR separates Line A in two different domains. At both sides of the SAR, two fault systems are seen, the Tuz Gölü Fault (TGF) and a thrust linked to it, the Şereflikoçhisar−Aksaray Thrust (SAT), reported here for the first time (Fig. 3.5).

These two prominent south-west dipping faults and a series of mainly west- (but also east-) dipping faults constitute the Tuz Gölü Fault System (TGFS). Figure 3.5 shows that these faults cross-cut each other and some were reactivated, as happened for the TGF (s. s.). This is seen in the western side of the fault system as a roll-over anticline and a harpoon-shaped inversion geometry. Other fault structures to the north-east of the TGFS depict minor horst shapes for the lower part of Unit 3. To the south-west of the TGFS, several normal faults offset all the Cenozoic sequence.

A 3 km-wide thickened area affected by diffuse extensional features is seen immediately to the south-west of the SAR, whilst to the north-east, the units are thickening toward it progressively. Unit 1 has maximum thicknesses of 250 m in the thickened area south-west of the TGF, and thins south-westward in a horizontal space of 5 km. On the other hand, nearly constant thicknesses of less than 100 m are seen for this unit in the north-eastern side of the SAT. Unit 2 wedges in toward the SAR and reaches its maximum thickness, ∼600 m, near the SAT. On the western side of the SAR, near the TGF, Unit 2 is two times thinner. Elsewhere along Line A, Unit 2 has thicknesses of some $50 - 200$ m. In a similar fashion as Unit 2, the distribution of Unit 3 shows relevant thickening toward the TGF and the SAT. The Unit 3 thickening is related to normal faults in the south-western thickened area, and is twice as thick in the north-eastern side of these structures. Unit 3 has average thicknesses of $\sim 100 - 400$ m and maximum thicknesses of some 1200 m, reached to the north-east of the SAT. The contact between the units 3 and 4 is evidenced in the north-eastern side of the TGF, with reflections marking an angular unconformity. The thickened structure seen south-west of TGF for the previous units is not repeated by Unit 4. Instead, a prominent south-westward−thickening wedge is seen along the entire profile. For Unit 4, the thickening of sediments occurs from the north-east to the south-west, from ±750 m to ca. 2800 m, and its base deepens from 1 km to 3 km in the same direction. Neither the Miocene units (unit 1 to 3), nor the Palæogene unit (Unit 4) have reflections that evidenced basin terminations.

Seismic line B

Seismic line B lies around 30 km to the SE of line A (Fig. 3.2). Similar to the line described above, this line crosses the TGF and the SAR. Even though sediment distribution and fault morphologies resemble those found in line A, some important differences are observed.

Three major extensional systems on the sides of the SAR are seen in line B (Fig. 3.5). These faults are the described south-west dipping TGF and SAT and a major deep-rooted normal fault dipping north-east. Together they form a horst that is mimicked by several smaller faults offsetting units from 2 to 5. A well-developed rollover anticline with a harpoon structure is seen on the south-western side of TGF. Other minor normal faults are observed, especially in the south-western side of the line.

Thickening of the Neogene package (units 1, 2 and 3) occurs toward the three major faults. These units have no basin-termination reflections on either side of the line. Close to the TGF to the south-west, Unit 1 shows a thickened area of about

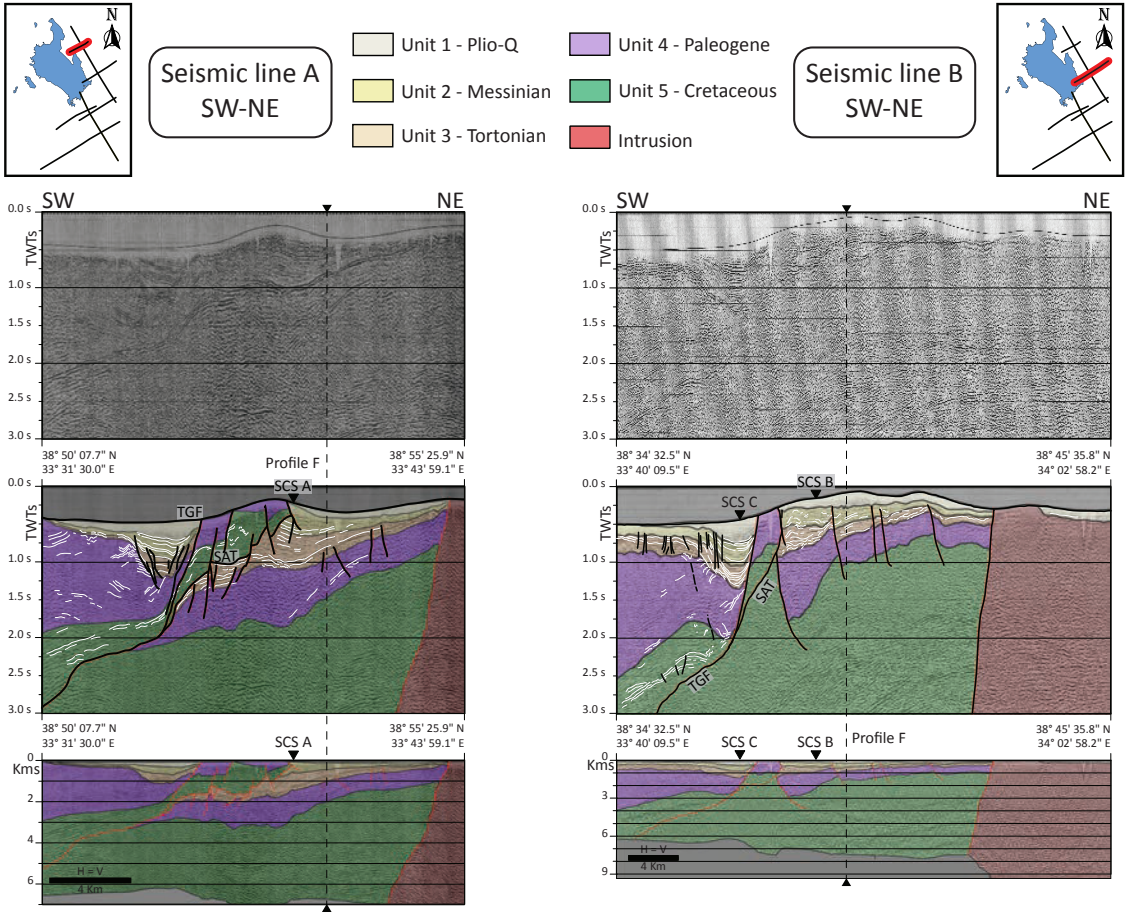

Figure 3.5: *Northern NE–SW oriented lines. Original seismic image, seismic interpretation in TWT and depth-converted profile for the lines A and B. Location map and intersection with other seismic profiles used in this study are also shown.*

400 m that thins toward the west from approximately 4.5 km to less than 50 m. To the north-east of the SAT, Unit 1 shows a ±15 km width shallow depression with a maximum thickness of around 250 m in its middle part. Deepening in the section, Unit 2 depicts similar thickness distributions as Unit 1. The thicknesses of Unit 2 are 1.5 times larger in the north-eastern side of the TGF with respect its south-western side. The thickened area is again seen on the western side of TGF, although thinning toward the south-west is not evident. Unit 2 maintains relatively constant thicknesses toward the south-west (around 200 − 250 m), but thins away from these fault systems in the north-eastern side. In a similar manner, Unit 3 thickens toward the TGF and the SAT. To the south-west of TGF, Unit 3 thicknesses reach some 700 m. Constant thicknesses of around 450 − 500 m are maintained for this unit toward the south-west. The shallowing of the base of Unit 3 while moving south-west away from the TGF ends within 3 km, where its base becomes horizontal. To the north-east, close to the SAT, Unit 3 thicknesses are ±650 m. Unit 3 thins toward the north-east to some 200 − 250 m in the north-easternmost part of the line. Wedging toward the south-west of Unit 4 is another a remarkable feature, with thicknesses ranging from ca. 500 m on the north-east of the line to ±3000 m on the south-west of it, where the base of Unit 4 deepens to ca. 3700 m.

Seismic lines C and D

Seismic sections C and D lie some 35 km SE of line B (Figure 3.6). These SW−NE oriented lines are shifted approx. 5 km in the NW−SE direction, with the north-eastern sector of line C and the south-western sector of line D depicting the same geologic features (Fig. 3.2). Therefore, these lines have been analysed together. The north-eastern side of line D ends inside the SAR, thus providing no information about the basin of that side of the high. The base of the Neogene units shows relatively constant depths, with two maxima associated with the main fault systems, the SFS in the west and the TGF in the east (Fig. 3.6).

The SFS is seen as two prominent south-west−dipping faults (profile C in Fig. 3.6) offsetting Unit 3, the middle part of Unit 2 of the Neogene package (approx. Upper Miocene), and several associated structures. In a similar manner, the TGF is a south-west dipping feature with several associated faults (profile D in Fig. 3.6). These faults show extensional as well as contractional features, but the harpoon structure is not well-defined. Considering its location, the easternmost fault of the line could be the SAT; however, the lack of reverse offset points to it being an extensional fault part of the TGFS. Extensional secondary faults accommodate as well the movement in the western side of the TGF.

Thickening of units 1, 2 and 3 to the north-east of the TGF is not seen. The Neogene units depict limited thicknesses on that side of the fault and the depth at their base is less than 500 m. Within the Neogene package, Unit 1 has a fairy continuous thickness with a maximum of 200 m. The thicknesses of Unit 2 are around 300 − 400 m and fairly continuous. The thicknesses of Unit 3 range from some 400 m to 600 m. When affected by the major structures, Unit 3 has maximum thicknesses of ±1000 m. The angular unconformity between Unit 3 and Unit 4 is clearly revealed in both profiles. Unit 4 reflections are irregularly deformed and show high dip angles (better seen in profile D). The bottom of Unit 4 seems to be deposited on an inherited palæotopography and shows large variations in depth

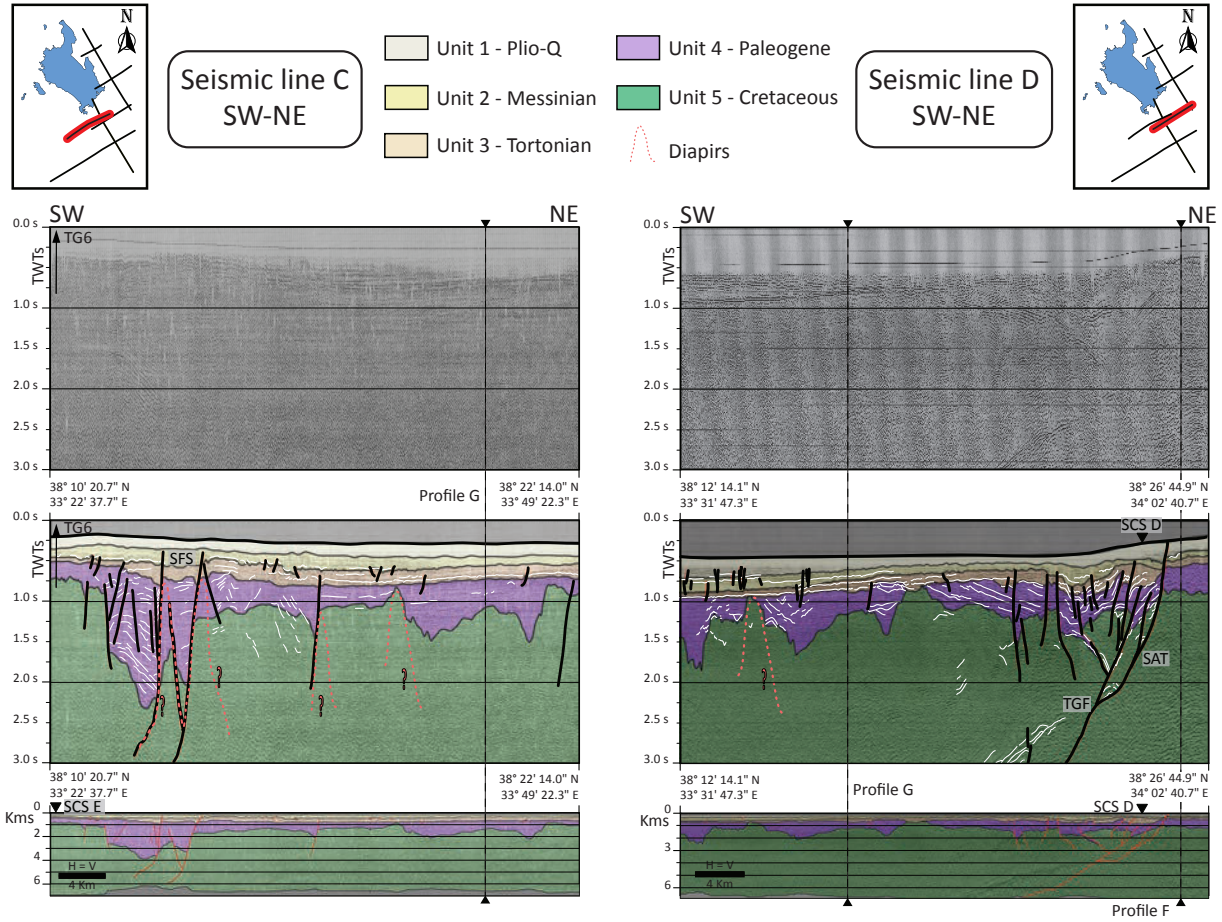

Figure 3.6: *Center NE–SW oriented lines. Original seismic image, seismic interpretation in TWT and depth-converted profile for the lines C and D. Location map and intersection with other seismic profiles used in this study are also shown.*

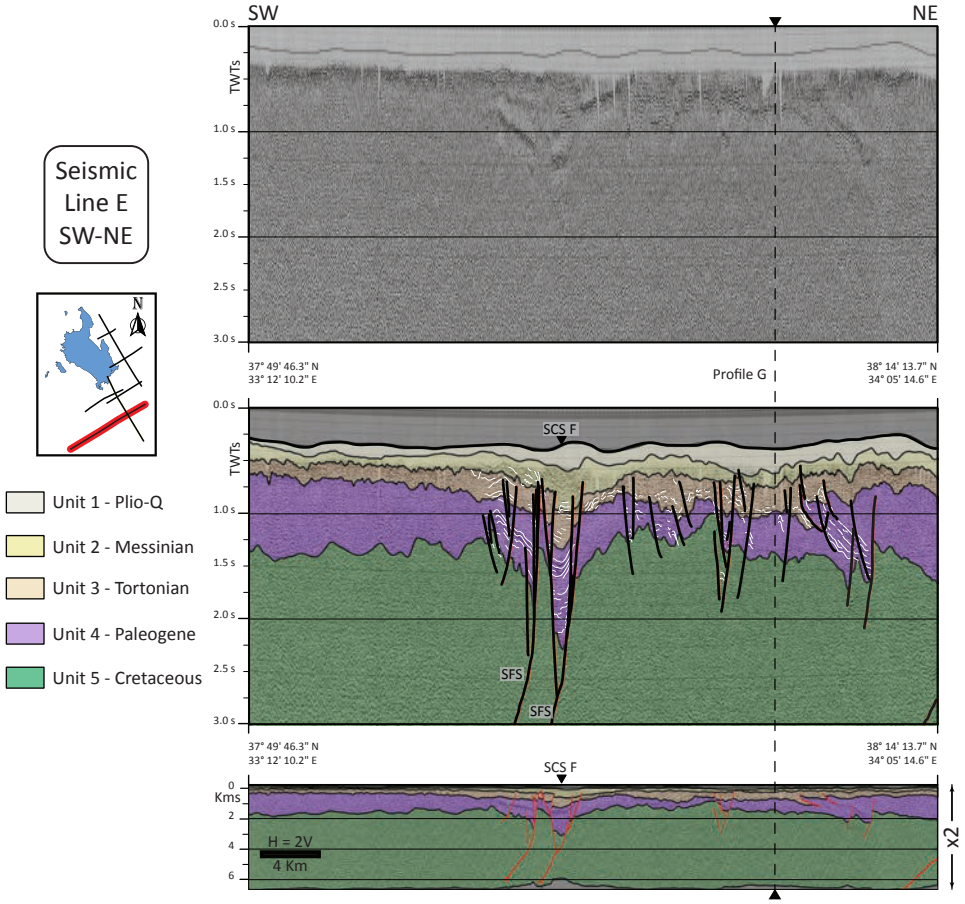

Figure 3.7: *Southern NE–SW oriented line. Original seismic image, seismic interpretation in TWT and depth-converted profile for the line E. Location map and intersection with other seismic profiles used in this study are also shown. Line shown with double vertical exaggeration.*

(from less than 1 km to circa 4 km). The combined action of salt diapirs in this area [Uğurtaş, 1975] and movements along the faults of the SFS might have caused the morphology observed in the south-west part of profile C. Thicknesses of more than 3 km are seen for Unit 4 in relation with the SFS.

Seismic line E

Seismic profile E is located some 30 km south-east of line D (Fig. 3.2). The north-east end of Line E ends close to TGF, while the SFS can be seen at its south-west (Fig. 3.7).

The most apparent structure seen in line E is the SFS, situated around the center of this line. The SFS is composed of two major south-west dipping extensional faults reaching the base of Unit 2 and at least two similar but relatively minor

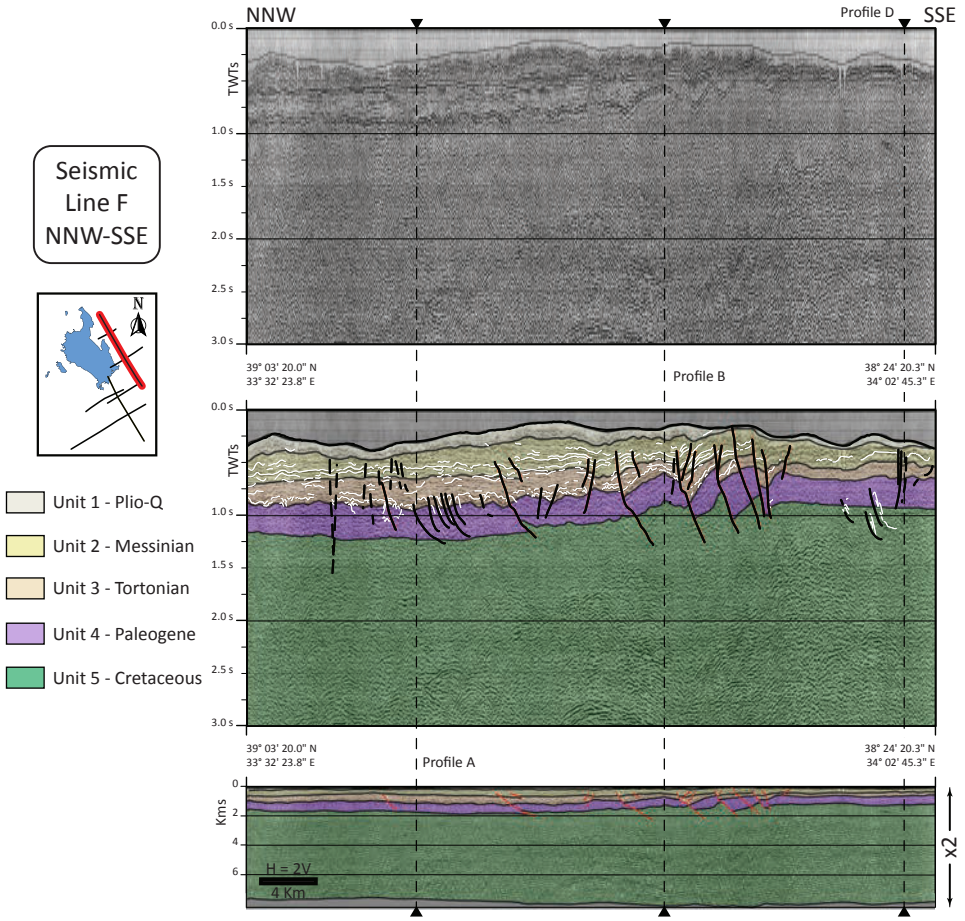

Figure 3.8: *Eastern NNW–SSE oriented line. Original seismic image, seismic interpretation in TWT and depth-converted profile for the line F. Location map and intersection with other seismic profiles used in this study are also shown. Line shown with double vertical exaggeration.*

structures toward the north-east. Numerous other secondary normal structures are found between the SFS and the north-eastern end of the section (Fig. 3.7). Units 1, 2 and 3 thicken when affected by the SFS and the other analogous structures. This thickening is seen for units 1 and 2 and reaches values of around 500 m for Unit 3. Unit 4 also shows thickening caused by the SFS. Toward the north-east end of the line, the thickening of Unit 4 indicates a proximity to the west side of the TGF.

3.4.2 The NNW–SSE-trending seismic sections

Lines F and G are oriented parallel to one another and shifted laterally ∼35 km. The southernmost area of Line F and the northernmost area of Line G are coincidental, and depict similar geologic features for ∼35 km. When both lines are taken together,

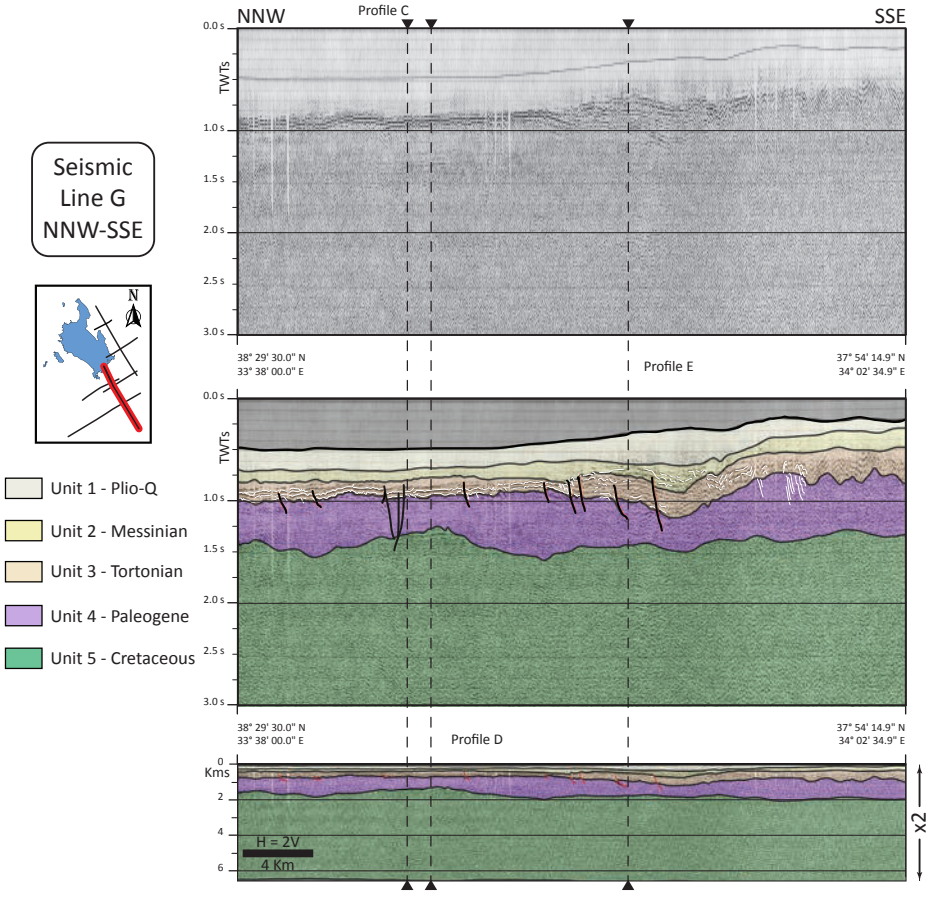

Figure 3.9: *Western NNW−SSE oriented line. Original seismic image, seismic interpretation in TWT and depth-converted profile for the line G. Location map and intersection with other seismic profiles used in this study are also shown. Line shown with double vertical exaggeration.*

they result in a ca. 170 km long section across the TGB parallel to the SAR. These lines share similar patterns and thicknesses of the seismic units and depict the same structures. Thus, they are here described together (Figures 3.8 and 3.9).

The thicknesses of the seismic units in profiles F and G are fairly constant. The reflections show no basin terminations within the extent of the lines. However, variations in the trend of these units are seen in both profiles. In line F, units 1, 2 and 3 thicken gently toward the NNW (Fig. 3.8). The base of Unit 4 in line F deepens toward the north from 1 km to 1, 5 km and is offset by several normal faults, especially in the middle to southern parts of the profile. Most faults are dipping south and have vertical displacements up to 500 m. Line G shows thickening for Unit 2, and especially for Unit 3, towards the SSE (Fig. 3.9). This western profile shows $1500 - 1700$ m continuous fairly horizontal depth for the base of Unit 4 and almost no disruption by faults.

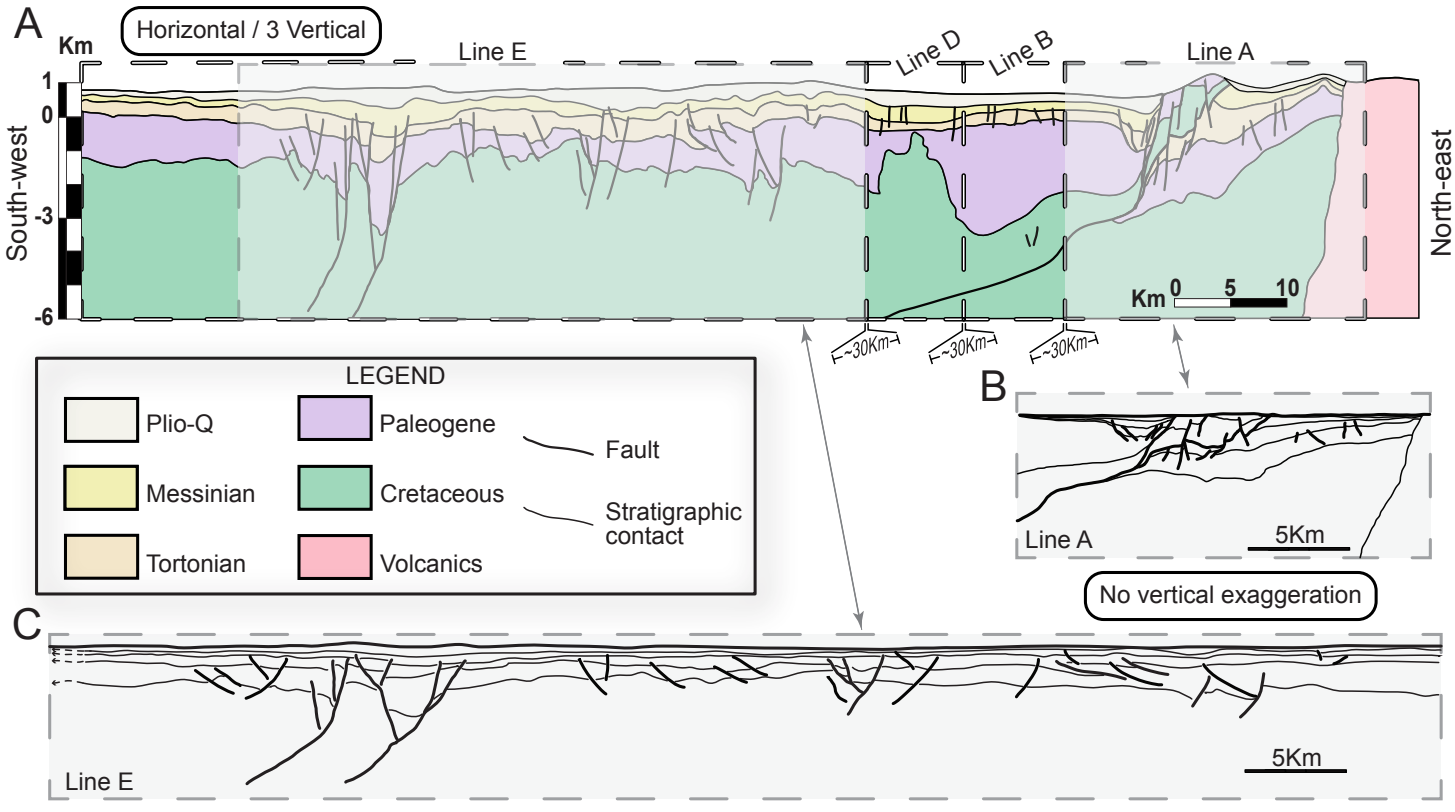

Figure 3.10: *(A) Composite cross-section showing the main structures found in the study area, transecting them perpendicularly to their main trends (SW−NE). This composite section is formed by four different seismic sections (from SW to NE, line E, line D, line B and line A) that are separated around* 30 km *from one another in the NNW−SSE direction. This profile is exaggerated 3 times in the vertical. (B and C) Depth-converted (scale 1:1) seismic interpretation of line A (used as input for the palinspastic restoration) and line E.*

3.5 3D architecture of the Tuz Gölü Basin

As observed in the lines, the Tuz Gölü Basin (TGB) presents small thickness variations for the main units in the NNW−SSE direction and more prominent ones in the NE−SW direction. In the NE−SW direction, the reflections in the upper section (uppermost 2 s) are pinching away both north-eastward and south-westward from the TGF and the SAT, but no clear basin terminations are seen on either side. Moreover, the pinching-out geometry is seen for the northern area but not in the southern part.

3.5.1 The composite section

A composite section has been constructed in NE−SW direction in order to represent overall sedimentary geometries and deformation structures (Fig. 3.10). As observed in this composite section, all the seismic units are continuous and the only disruption is in correspondence with the SAR, the SFS, and associated faults (Fig. 3.10).

The Plio-Q unit (Unit 1) thickens in three diferent areas, the SFS, the TGFS and in relation to a secondary fault system in the center-left of the composite section. In contrast, units 2 and 3 show only two main depocenters. Units 2 and 3 are thickest in correspondence with the western side of the SFS and the TGFS, showing wedges at their western and eastern sides (see Fig. 3.10). The position of the base of Unit 4 has important variations, from less than 200 m to some 4 km depth. Starting in the north-eastern part of the study area (see Figs. 3.2 and 3.10), Unit 4 shows growing thicknesses south-westward, with a maximum of approx. 3 km. This thickening is disrupted when moving toward the south-west along the composite section by either a palæohigh or, more probably, a salt diapir. Unit 4 thins in this area to values of $500 - 800$ m, remains fairly continuous in the south-westernmost area and thickens again to approx. 2.5 km in the SFS. The seismic units are continuous and the reflections show no basin terminations along the composite section.

Several secondary structures accommodated the movement imposed by these systems, thus having analogous sediment relationships and orientations but smaller offsets. Other minor contractional as well as extensional faults affect units 2, 3 and 4, indicating a variety of events. The only seismic-scale folds seen are exclusively associated with fault movements.

The Şereflikoçhisar−Aksaray ridge (SAR)

The relief of the SAR, up to 250 m in variation, is the morphologic expression of the structures found underneath it, as observed in the seismic images. Under the SAR, the TGFS is a compound of four different fault families. There are two deep-rooted normal faults with opposite dips that create the main horst morphology. The TGF, which bounds the SAR to the south-west, is one of these faults. The SAT, linked with the TGF at depth, is a top to the north-east thrust outcropping Palæogene and Cretaceous rocks in the core of the SAR and bounding it to the north- east. We also observe a series of extensional faults in the hangingwall of the TGF, thickening the Miocene sequence, and a second set of normal faults in the north-east side of the system, which are parallel to the primary structures and cut the thrust sheet. The cutting relationships amongst these fault families show three deformation phases.

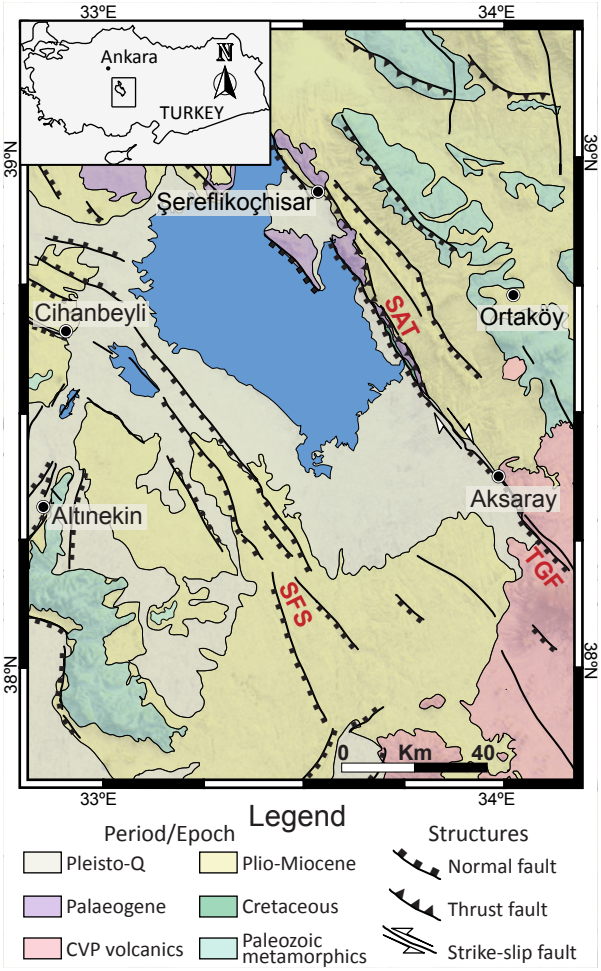

Figure 3.11: *New structural map for the study area. Corrections on the location of several structures and on the sense of movement are made on the base of the analysis of the interpreted seismic refraction lines and* 1 arc *DEM and LandSat 7 images set from the NASA. Modified after maps by Dirik and Erol [2000]; Özsayın and Dirik [2007].*

The older TGF extensional system is transected by the SAT, which is in turn cut by a younger, stratigraphically higher system of normal faults. This clearly indicates a sequence of extension-shortening-extension events.

Sultanhanı fault system (SFS)

The major structures found in the SFS (Fig. 3.10) are two normal south-west dipping faults involving basement. These two faults double the thicknesses of the Palæogene unit and affect both units 2 and 3. It was observed that the SFS is sealed by the upper part of Unit 2. The displacement and geometry of the different rock units offset by the SFS indicate initiation of the system by Late Cretaceous times. On the eastern side, several mimicking structures closely resemble the morphology of the SFS, affecting the upper and lower boundaries of the Palæogene unit. The fault system behaved as a right lateral transtensional fault zone in Miocene and as a normal fault in Pleistocene [Özsayın and Dirik, 2011].

3.5.2 The structural map

Integrating literature data [Dirik and Erol, 2000; Özsayın and Dirik, 2007, and the references therein] with the new observations found in the seismic lines and the analysis of 1 arc DEM and LandSat 7, an updated structural map was constructed for the study area (Fig. 3.11).

A NW−SE orientation of the major structures is clearly seen in this structural map. Most of the structures found in the area are extensional in character, with the exception of the SAT. The two main fault systems, the TGFS and the SFS, are laterally continuous structures. As observed in the structural map, the TGF and SAT components of the TGFS diverge north of Aksaray, limiting Palæogene and Cretaceous rocks to a narrow elongated area. The north continuation of the SFS widens into the Inönü-Eskişehir Fault System [Özsayın and Dirik, 2007].

3.5.3 The isochore maps

In order to understand the sediment accumulation patterns and the thickness distributions of the area, two isochore maps were made for units 2 and 3 representing the vertical sedimentary thicknesses. Isochore maps are constructed by subtracting the upper and lower boundary surfaces of each unit. Therefore, the isochore maps represent equal true vertical thicknesses of the unit, and are coincident with isopach maps only in horizontal layers. Precision on the thickness estimation depends primarily on the confidence of the seismic correlation of the base and the top of the target unit, which is variable but at a maximum for units 2 and 3. Another factor influencing the accuracy of the isochore maps is the extrapolation method used (krigging). The effects produced by the extrapolation were partially corrected using a specified anisotropy of 325° N, i.e. giving higher statistic load to values oriented parallel to the elongated trending of the basin, and by manual reinterpretation and correction of artefacts. Both maps show the present-day disposition of the sediments, without accounting for the distortions created by the main structures in the area (Fig. 3.12).

The Unit 2 thickness accumulations show two different depocenters (Fig. 3.12-A), both NW−SE oriented; in the north-east and in the south-west. The north-eastern depocenter is divided in turn in two depressions on both sides of a NW−SE relative high, which corresponds to the SAR. Sediments to the west of this high cover a narrower area and are thinner than those lying in the eastern counterpart area. The presence of the TGF and the SAT might have been important by this time period, as seen by the development of the two differentiated depressions. The second depocenter, in the south-west, is broader than the former. In Unit 2, sediment vertical thicknesses are maximum in this depocenter and reach some 500 m.

The isochore map for the Unit 3 (Fig. 3.12-B) depicts two areas of strong accumulation (reaching 800 m and more than 900 m). Separated by a relative positive oriented NE−SW, these areas are striking broadly in NW−SE and NE−SW directions, respectively. The northernmost depocenter is elongated and located in alignment with the structural high seen for the Unit 2. The south-western depocenter is shallower and broader than the northern depocenter. This area of low sediment accumulations might be a consequence of an inherited structural high located approximately parallel to the southern depocenter and might have forced NE−SW orientated deposition in it. This broad area of deposition is as well affected by minor highs.

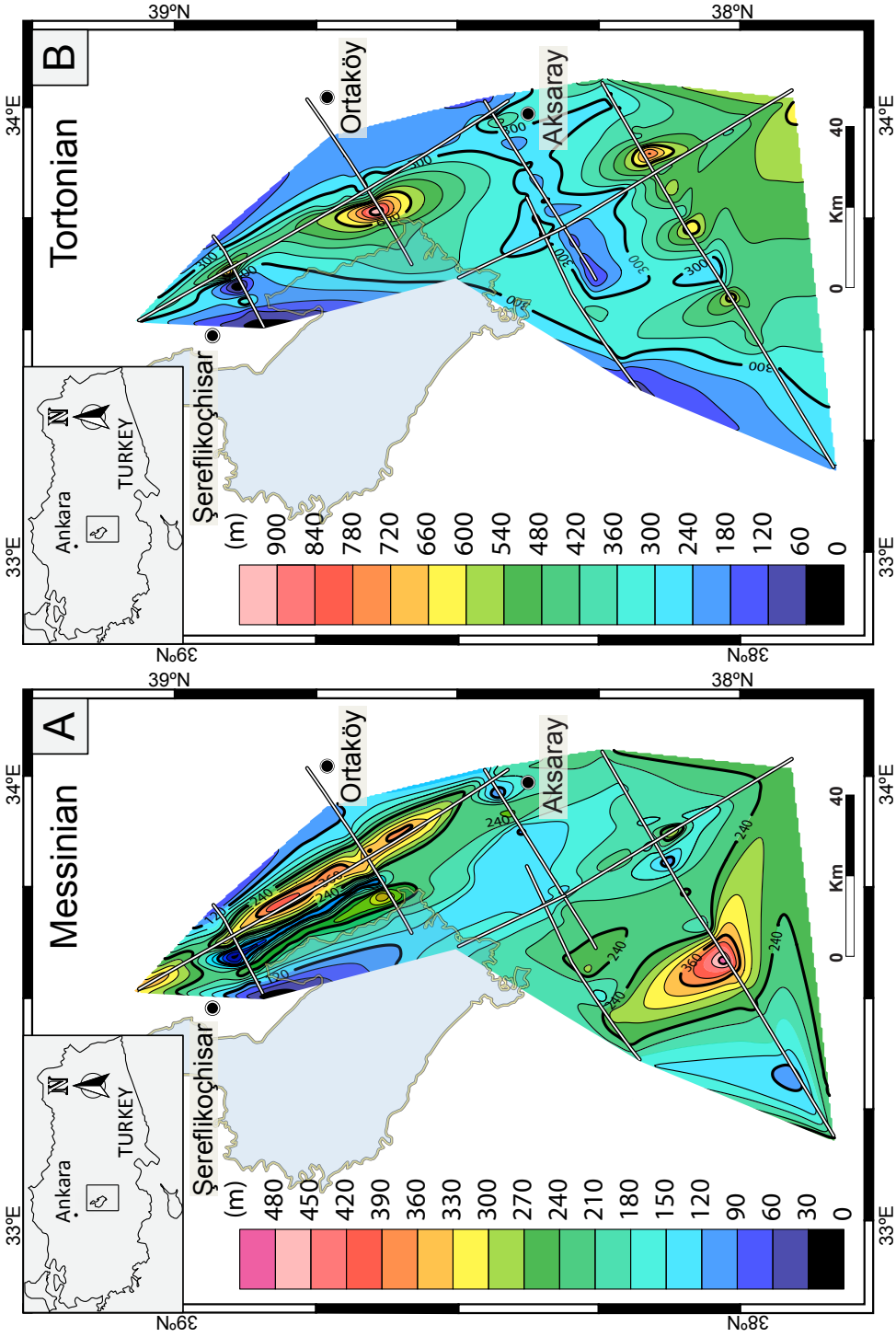

Figure 3.12: *Isochore maps showing thicknesses distribution of Unit 2 - Messinian (A) and Unit 3 - Tortonian (B). The thickness is represented in meters in the colored area to the left of each figure. The location of the seismic lines is also shown.*

Comparison of these maps shows wider trenches of sedimentary accumulations for the Unit 2 and narrower for Unit 3. The distribution of thicknesses seen for Unit 2 sediments, i.e. the differentiation of areas with small thickness accumulations that do not coincide with analogous features observed for younger times, indicates the probable presence of pre-Tortonian topography.

3.6 Tectonic motions in the Tuz Gölü Basin

3.6.1 Vertical movements

Methodology and data

We created six backstripped subsidence history plots for six localities corresponding to five synthetic wells obtained from the depth-converted sections, called subsidence curve sites *(SCSs)* A to E, and one to the Tuz Gölü 6 well (*SCS* TG6)(Table 3.1). The sites were chosen in areas where the reliability of the seismic horizons was maximum and meaningful sediment thicknesses were found (Fig. 3.2).

Table 3.1: *Compacted thicknesses as measured on the synthetic wells and TG6 well*

Sites	**Seismic units thickness (m)**			**Elevation**
	Unit 1-Plio-Q	Unit 2-Messinian	Unit 3-Tortonian	**a.s.l. (m)**
SCS A	120	330	550	1030
SCS B	150	350	500	1175
SCS C	375	425	480	900
SCS D	150	200	200	930
SCS F	170	450	620	1050
SCS TG6	340	244	199	1000

To produce the subsidence curves, information on absolute sea level fluctuations and paleobathymetry is needed and the measured thicknesses need to be decompacted (see Chapter 2). Since the vast majority of the Tertiary to Quaternary sediments in the area are lacustrine to fluvial and palæoaltitude information was not available, water-depths were considered zero and do not necessarily correspond to sea level. Total decompacted thicknesses were calculated applying the approach by Steckler and Watts [1978], using standard mean, maximum and minimum porosity-depths functions [Bond and Kominz, 1984b; Bessis, 1986b; Mavko et al., 2003], and average decompaction values [Sclater and Christie, 1980] (Table 2.1, Chapter 2).

In other to correct the effect of compaction, simplified lithologies have been assigned to each defined unit (Table 2.1 in Chapter 2), allowing for the definition of porosity and density as a function of depth. Proceeding in this manner, one by one decompaction of each package was subsequently produced along the minimum and the maximum porosity-depth curves. To construct the tectonic subsidence, the density of the entire sedimentary column is calculated and the depth of basement is corrected for the sediment load assuming Airy isostasy (mantle density of 3.3 g/cm^3).

We have limited our analysis to the Tortonian-Recent interval. The later upward movement shown in the plots is the result of adding the present day topography to

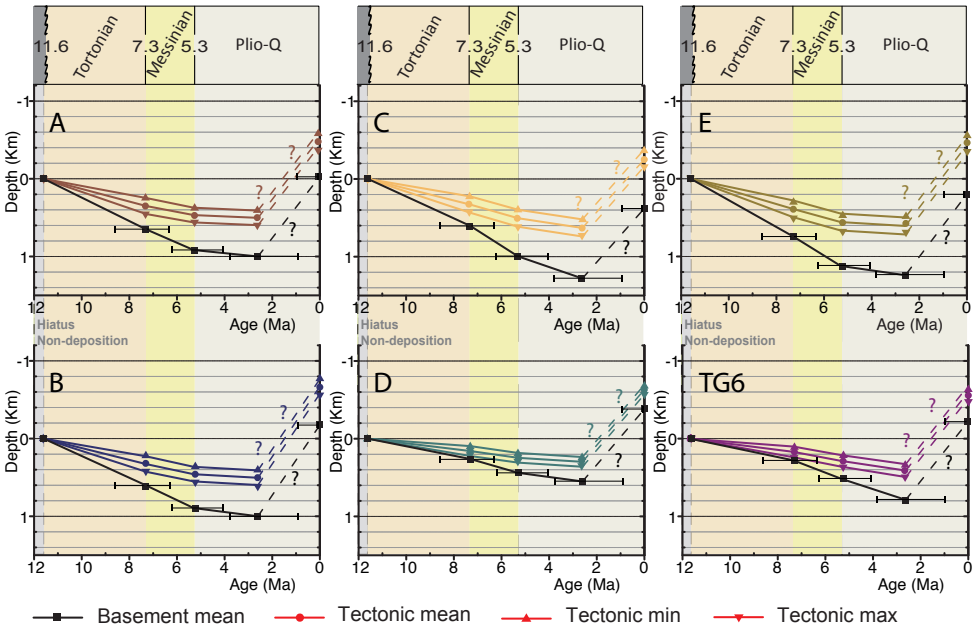

Figure 3.13: *Subsidence curve plots for the synthetic wells (SCS A-to-E) and the TG6 well (SCS TG6). Location of these sites are shown Fig. 3.2. The initial topography is assumed to be* 0 km *in all cases. The upward motion (positive slope) observed in the younger stages is created by including the value of the present day topography to the curve, thus bringing the curves to their present depths.*

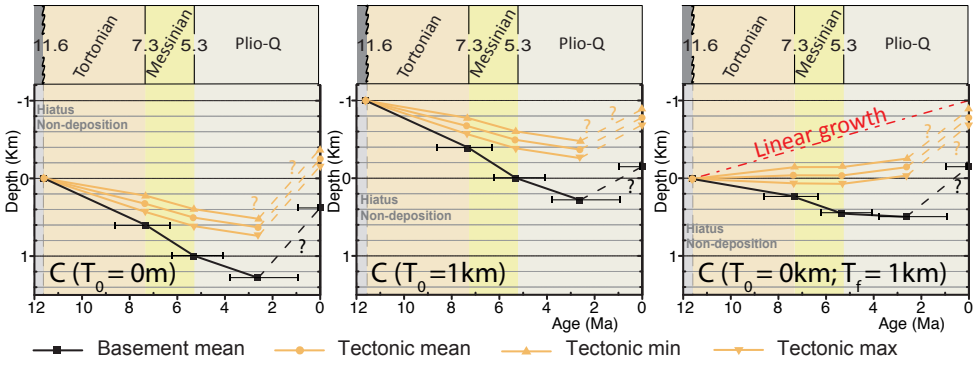

Figure 3.14: *Scenarios with different initial palæoelevations. Left panel is the reference scenario, SCS C, in which initial topography is considered as 0 km and younger uplift corresponds to present day depths of the points in the curve (see Fig. 3.13). The central panel corresponds to a scenario in which the initial palæoelevation has been considered to be similar to present topography (*1 km*) since Tortonian times, for the SCS C. The panel to the right represents an scenario in which a linear topographic growth is assumed from Tortonian (*0 km*) to present (*1 km*), for SCS C.*

the curve and has no tectonic meaning. To further understand the role of absolute elevations during basin development, we investigated different scenarios.

Analysis of vertical motions

All subsidence plots (Figure 3.13) show continuous subsidence for the Upper Miocene times and part of the Pliocene, with fairly constant basement subsidence rates. Relatively similar trends are depicted for all the subsidence curve sites (*SCS*), i. e., subsidence rates are more pronounced during Miocene times and decrease during early Pliocene (see Fig. 3.13).

However, some small differences amongst the chosen sites can be observed. *SCS* C, in the hangingwall of TGF, shows a high and almost continuous subsidence rate throughout all the Miocene and the Early Pliocene (0, 14 mm/y for both periods). Contrarily, the other site located in TGF hangingwall, *SCS* D, shows continuous low rates (0, 064 mm/y). *SCS* A and B, in the footwall of TGF, show intermediate values for the Miocene that decrease in Pliocene times (as low as 0, 044 mm/y for *SCS* A). *SCS* E, located in the hangingwall of SFS, shows the highest rates (0, 17 mm/y) during Miocene times, which decrease considerably during Early Pliocene. In contrast, in SFS footwall, the *SCS* TG6 show low rates of basement subsidence in the Miocene and the highest subsidence rates (0, 063 mm/y) for Early Pliocene times.

The primary subsidence signal observed for all the subsidence curves indicate continuous regional subsidence in the area during Tortonian-Early Pliocene times. A relevant initial subsidence period took place in Tortonian or earlier times. During this initial phase, a NE-SW elongated area, comprising the *SCS* D and *SCS* TG6, remained at a higher position. Subsequent lower subsidence rates occurred in Early Pliocene times. The relevant subsidence rates seen for both periods in *SCS* C might be in association with continued activity of the TGF. It is worth mentioning that both sides of the TGFS (NE-SW direction) show similar subsidence curves (see *SCS* A and B) but relevant differences are seen between the northern (*SCS* A, B and C) and southern sites (*SCS* D) along the strike of this system.

Scenarios of absolute elevations

The values of subsidence depths obtained for the reference scenario *SCS* C, discussed above, were compared with two different palæoelevation scenarios to consider the influence of the palæotopography (Fig. 3.14). Scenario 1 assumes that a palæoelevation equal to present day topography (which we have considered ∼1 km) existed since Tortonian times. In Scenario 2 the palæoelevation gradually grows from 0 km in Tortonian times, when subsidence initiated, to 1 km at present times.

In Scenario 1 (central panel), *SCS* C reaches sea level depths by Late Miocene and Pliocene times. This signal is an indication that the sediment accumulation accounted in the study area is unlikely to result from palæotopograhy infill and may rather be a consequence of tectonic-driven subsidence. However, in this scenario, *SCS* D and the *SCS* TG6 would have remained above sea level. This implies that the *SCS* C and *SCS* TG6 were probably parts of elevated terrains (presently coinciding with the areas of TGF and SFS), while overall tectonic subsidence occurred.

In Scenario 2 (right panel), the tectonic basement curves remain at sea level during the subsidence period due to the effect of the progressive uplift. The basement

curve remains constantly under the sea level, and it reaches values of some 500 m by Pliocene. The subsidence curves in this scenario represent a situation in which the contribution to subsidence by tectonic forces is minimum or absent and the contribution by sediment loading might be the driving mechanism.

3.6.2 Horizontal movements

Methodology and data

The depth-converted seismic line A (Fig. 3.5) was used for restoration (see Chapter 2). Line A transects at a high angle the major structures accounting for horizontal displacements in the area and it is roughly parallel to the transport directions obtained by [Özsayın et al., 2013] and in agreement with other studies in surrounding areas [e.g. Koçyiğit et al., 1995]. This line was simplified and divided into straight-lined blocks and faults, and faults with horizontal offsets <50 m were removed. Manual restoration was accomplished by mean of the equal area method described in Mitra and Namson [1989] without key-bed balanced modification. During restoration, fault geometries and block sectional areas remained constant (Fig. 2.2.2).

Restoration procedure

The retro-deformation was completed along fixed faults in a sequence opposite to the main transport direction, i.e. from north-east to south-west. Three different points along the section were used as reference to trace horizontal displacements. From north-east to south-west, they are *P(r)* in the stable area in the east, used as pin, *P(I)* on the hangingwall of the Şereflikoçhisar−Aksaray Thrust sliver and *P(II)* on the hangingwall of the Tuz Gölü normal fault in the west (Fig. 3.15, Chapter 2).

Restoration to pre-Miocene deposition was accomplished in eight steps by means of simple shear displacement (either vertical or ranging from 45-60° opposite to transport direction) (Fig. 3.15, Table 3.2).

Vertical shear along the end points of the section allowed restoration to a regional datum (from section I to section II in Fig. 3.15). To retro-deform the section to the moment of initial deposition of the Unit 1 (from section II to section III in Fig. 3.15), five block displacements along faults were performed. First *(1)*, vertical simple shear along the easternmost part of the section removed the Pliocene layer. Since the faults used to retrodeform steps *(2)* to *(4)* were transecting the SAT sheet, this structure was used as reference level. Rotational movements along the faults lead to restoration in *(2)* and *(3)*, and simple shear with 60° along the fault restored *(4)*. Restoration of the movement along the TGF, *(5)*, was accomplished by simple shear with 45° with respect to the horizontal. Retro-deformation to initial deposition of Unit 2 was achieved from section III to section V in Figure 3.15. Since the SAT is cutting Unit 2, the restoration along this fault in step *(6)* should be performed prior to the restoration of deposition of the mentioned unit. A 45° simple shear along the SAT leads to best retro-deformation results. This 45° simple shear was applied individually to each segment of the SAT. Oblique simple shear of 45° along the TGF in *(7)* retro-deformed the Unit 2. Final restoration along the TGF occurred by oblique simple shear of 45° for the Unit 3 in *(8)* (from section V to section VI), removing the last components of extension in the TGF.

The strain values obtained during restoration are shown in Table 3.2.

Table 3.2: *Horizontal displacements and strain from the restoration. TGF stands for Tuz Gölü Fault and SAT for Şereflikoçhisar−Aksaray Thrust. P(r) is the point of reference during restoration, and P(I) and P(II) are points located in the front and the back of the thrust. β is obtained dividing the final length against the initial length when measuring the distance P(r) - P(I) and P(r) - P(II).*

	Horizontal deformation				
	Displacement (m)		$\beta = l_1/l_0$		**Restored**
	P(I)	**P(II)**	**P(I)**	**P(II)**	**structures**
Base Pliocene	120	0	1.012	1	Small faults/TGF
Top Messinian	-8370	-8275	0.535	0.286	SAT
Base Messinian	85	0	1.005	1	TGF
Base Tortonian	55	0	1.003	1	TGF

Analysis of the horizontal motions

A primary analysis of the horizontal displacement along the Line A shows that this section was 8 km longer than present before the beginning of deposition of the Unit 3 sediments (Fig. 3.15). During deposition of Unit 2 (Fig. 3.15-IV), the line gained 140 m more in length, due to extension along the post-Palæogene TGF. Sometime before deposition of the Unit 1 sediments (Fig. 3.15-III), the emplacement of the SAT leads to more than 8 km of contractional horizontal displacement for both *P(I)* and *P(II)* with respect to *P(r)*, by far the most important displacement found during restoration. In the younger stages, horizontal displacements along TGF caused the removal of 120 m of extension, as quantified in the displacement of *P(II)*.

Restoration artefact and vertical motion mismatch

Our restoration for the movement along the SAT the the Late Miocen pre-base of produced a mismatch with the vertical motions quantified by the subsidence curves. Restoration of Line A produced in the south-west part of the TGF (blank area in Fig. 3.2-IV) a vertical displacement of some ∼2,8 km. The *SCS* C, in Line B, located as well in the hangingwall of the TGF and considered to have a similar evolution, indicate circa 1,3 km. This difference, produced by our decision to maintain block motion along the SAT, may be a consequence of any or a combination of the following; *(i)* the SAT transport direction is not north-east, *(ii)* the overall south-west tilt of the area and/or *(iii)* the volume changes caused by compaction (that could account for volume changes up to 40% [see Wood, 1981]).

We consider that palinspastic restoration is not a technique meant to account the vertical movements but to determine the horizontal displacements. Thus, we understand the primary horizontal signal seen in the restoration as factual. In this manner, here and elsewhere, values for the horizontal motions are obtained from the restoration and values for the vertical motions from the subsidence curves.

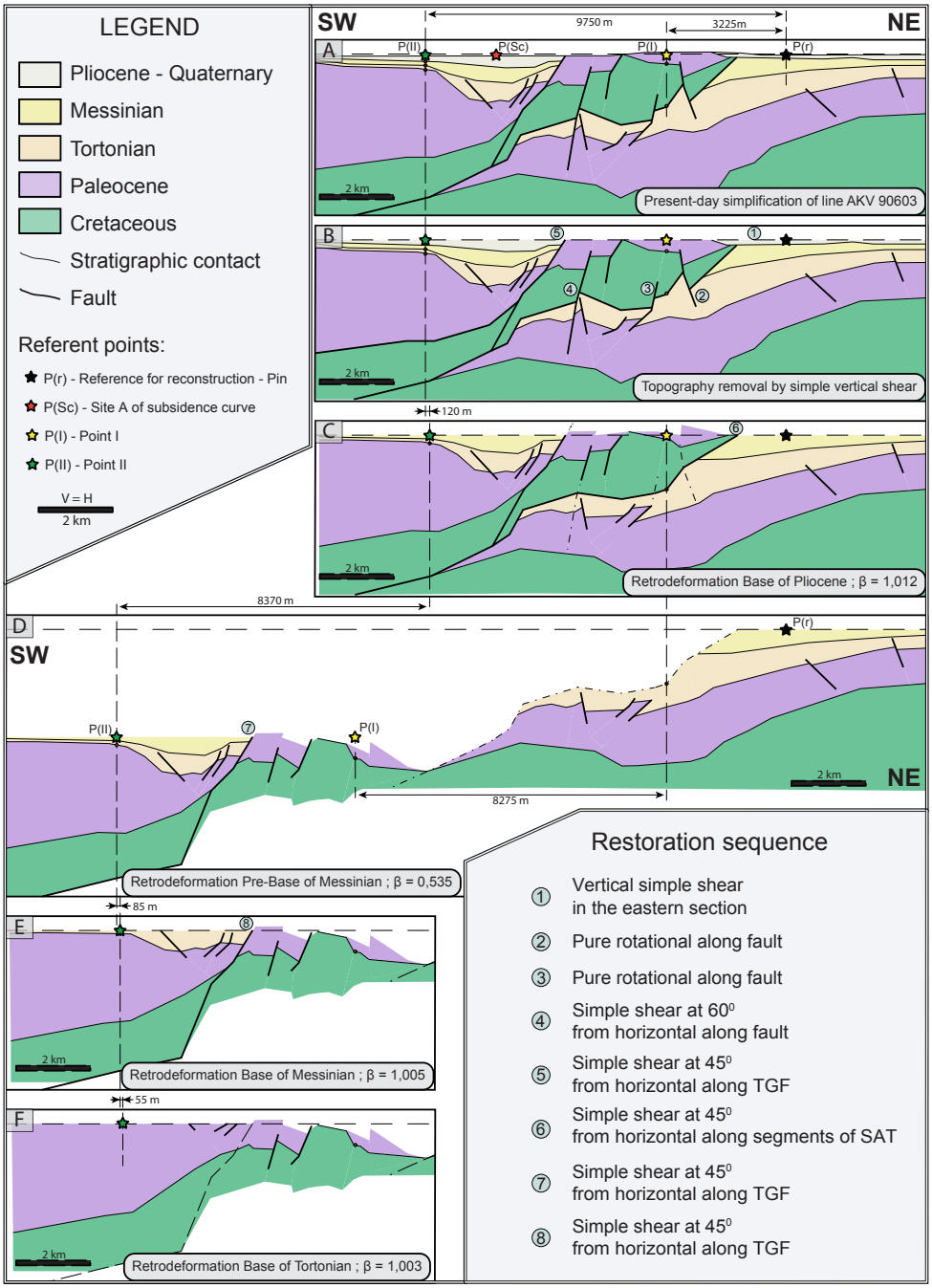

Figure 3.15: *Equal-area restoration of Line A and removal of each seismic unit for every time-slide until pre-Tortonian. The restoration sequence is performed in the order shown by the grey numbers both in the sections and in the lower right corner.*

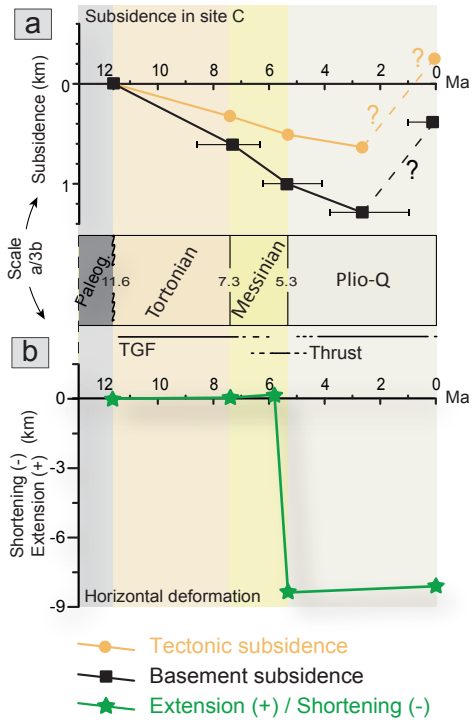

Figure 3.16: *Comparison between the subsidence curve in site C and values obtained during restoration as well as a tentative representation of activity of the main faults through time.*

3.6.3 Comparison of tectonic motions

The horizontal deformation values obtained in the restoration shown in Table 3.2 are plotted in Fig. 3.16, along with the subsidence curve in *SCS* C, and the estimated periods of activity on the main faults, for comparison.

No direct relationship can be established between subsidence curves and fault activity (see Fig. 3.16). During the beginning of post-Palæogene times, the initial movements on the TGF assumed 140 m of extension and subsided circa 600 m. Nevertheless, subsidence rates remained constant while subsequent SAT tectonics occurred. In this manner, ∼200 m of subsidence are linked with ∼8 km of shortening. One probable explanation is that overall subsidence happened in the area independently of the applied stresses. This is, both extensional and contractional phases occurred in the region whilst independent regional subsidence led to 800 m of downward motion.

3.7 Evolution of the Tuz Gölü area: A 3D model

3.7.1 Late Palæogene

Overall subsidence began in Maastrichtian times [Görür et al., 1984; Çemen et al., 1999], leading to the development of a broad sag basin that further developed during the Early Palæogene. In less than 13 Ma, the area experienced between 1500 m and 2200 m of basement subsidence (Fig. 3.17) with respect to the surroundings. The

extent of this basin exceeded the limits of the study area and its formation was not related with the development basin-forming faults. However, the SFS was active as an extensional or strike-slip intra-basinal fault during this time interval suggesting at least local extension.

After this subsidence phase, a long period of non-deposition settled, which is represented as an unconformity. This period is associated with regional uplift between 40 Ma and 23 Ma Genç and Yürür [2010], and shallowing and sea retreat in Central Anatolia by the end of the Lutetian [Çiner et al., 1996; Görür et al., 1998].

3.7.2 Late Tortonian

Sedimentation restarted by Tortonian times (Fig. 3.18). The previous regional subsidence in the sag basin changed toward a more structurally (fault) controlled subsidence. Both the TGFS and the SFS were active structures and clearly influenced the sediment distribution in the TGB. Trending in a NW−SE direction, the initial accumulation of sedimentary deposits in the north reached thicknesses of 800 m in relation with two extensional faults shaping a horst, namely the TGFS. Syntectonic deposition of Tortonian sediments at each side of this horst took place. The southern depocenter, striking in NE-SW direction, accumulated more than 900 m of sediments in relation with the SFS, where syntectonic deposition doubled the sedimentary thicknesses.

3.7.3 Late Messinian

A similar evolution to that occurring in Tortonian times happened in the area during the Messinian (Fig. 3.19). Continuation of subsidence and local extension led to further narrowing of the depocenters as markedly NNW−SSE oriented, in association with the activity of the TGFS and SFS. The depression related to the SFS accumulated up to 500 m of sediments (relative to the surroundings) during this period. Concurrently, 400 m of sediments deposited in relation to the TGFS. During continued subsidence, a latest Miocene-Pliocene shortening phase took place. This kinematic changeover resulted in the development of contractional features in the area. The SAR is the most relevant amongst these structures and was formed by the north-east emplaced SAT sliver, which accounted for more than 8 km of horizontal displacement.

3.7.4 Present

By the beginning of deposition of Pliocene sediments (Fig. 3.20), a new extensional phase followed the previous contraction [Özsayın et al., 2013]. We observe this on both sides of the TGFS; on the eastern side of the system normal faults offset the SAT, whereas in the western side a roll-over anticline morphology with an harpoon structure is found (Figs. 3.5 and 3.6). The development of this extensional reactivation accompanied the regional uplift of the area.

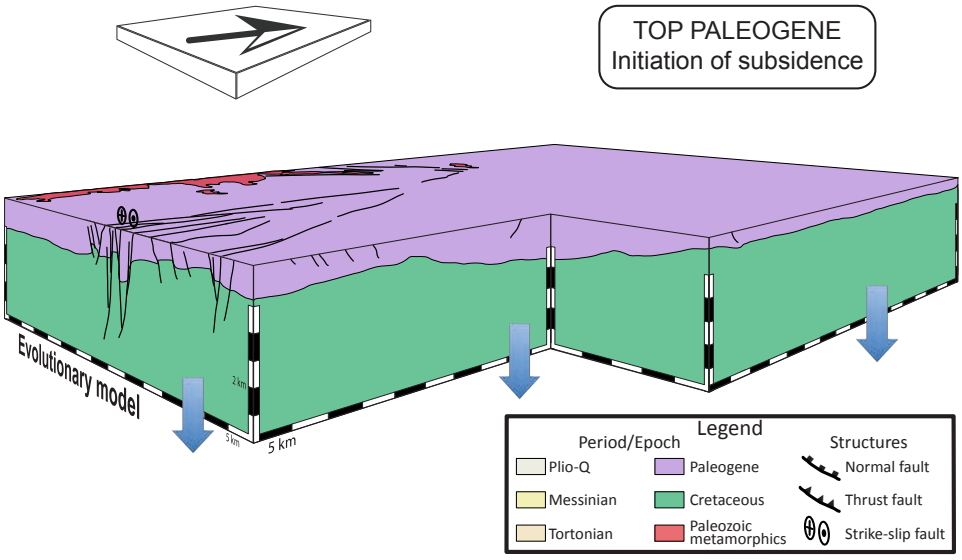

Figure 3.17: *Real-scale box-model (exaggerated three times in the vertical direction), showing the main tectonic structures and tectonic movements after Palæogene deposition. Arrows indicate direction, type and relative magnitude of movements.*

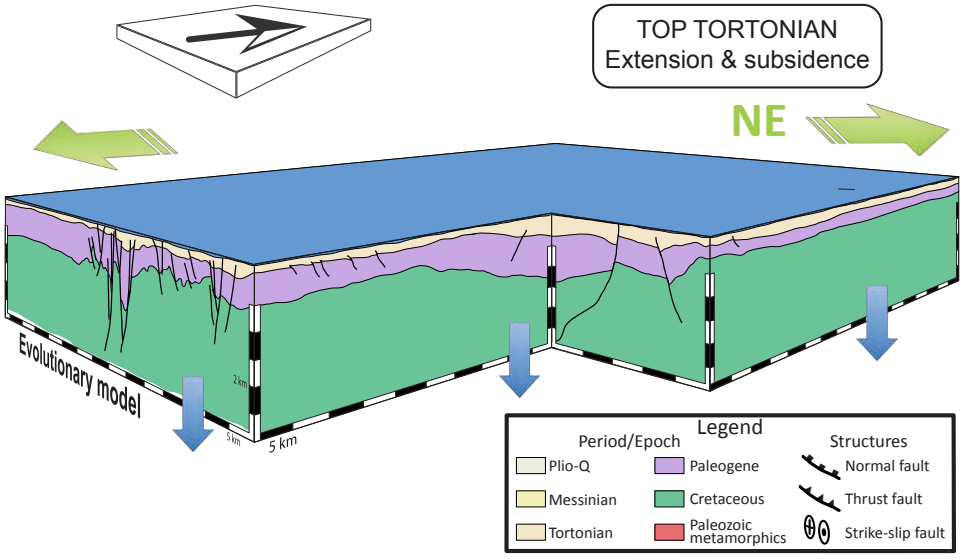

Figure 3.18: *Real-scale box-model (exaggerated three times in the vertical direction), showing the main tectonic structures and tectonic movements after Tortonian deposition. Arrows indicate direction, type and relative magnitude of movements.*

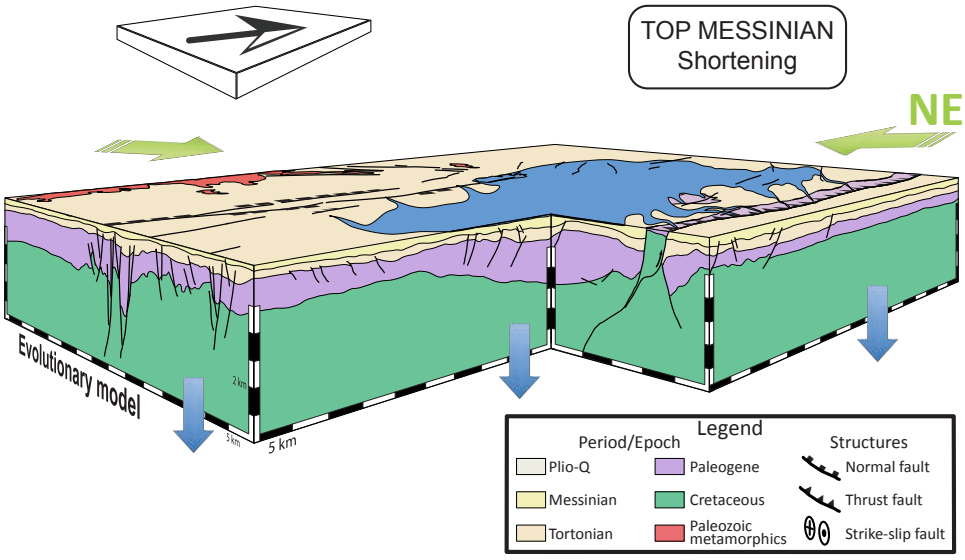

Figure 3.19: *Real-scale box-model (exaggerated three times in the vertical direction), showing the main tectonic structures and tectonic movements after Messinian deposition. Arrows indicate direction, type and relative magnitude of movements.*

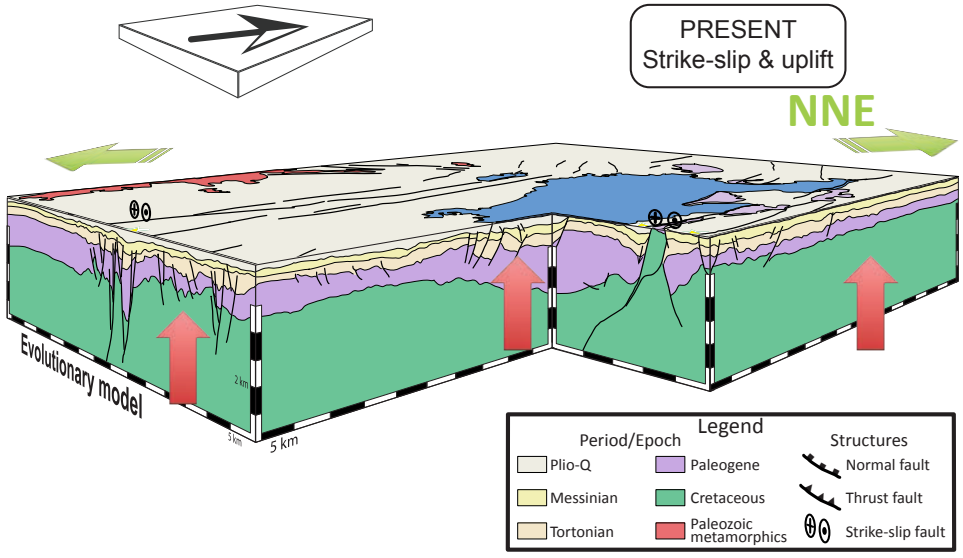

Figure 3.20: *Real-scale box-model (exaggerated three times in the vertical direction), showing the main tectonic structures and tectonic movements in Present times. Arrows indicate direction, type and relative magnitude of movements.*

3.8 Discussion

3.8.1 Extent of the Tuz Gölü Basin

The relevant literature on the area consider the TGFS and the SFS as Late Cretaceous to Palæogene basin-forming faults [e.g. Dirik and Göncüoğlu, 1996; Derman et al., 2000; Dirik and Erol, 2000; Özsayın and Dirik, 2007; Huvaz, 2009]. However, this seismo-structural study shows no basin terminations, and thus connection to or disconnection from other areas farther away could not be established. In the case of the TGFS, our palinspastic restoration demonstrates that this system was not present by Palæogene times. This interpretation is compatible with the thickness of Palæogene sediments which continuously increase from NE to SE disregarding the younger TGFS. Furthermore, the offsets shown indicate that the initial sedimentation is unrelated to the fault system and only partially affected by it at a later stage, which is at least as late as post-Palæogene. The SFS, a southward continuation of the Inönü-Eskişehir Fault System [Özsayın and Dirik, 2007], has been considered to be the east-dipping western boundary of the TGB or a fault pair shaping a graben [e.g. Dirik and Erol, 2000; Genç and Yürür, 2010]. However, within the area transected by the seismic lines, the SFS is shown as a south-west dipping fault set. This fault system was possibly present by Late Cretaceous times but created no boundary for the basin (Fig. 3.11). Instead, the SFS was probably acting as an extensional to strike-slip intra-basinal fault (see Fig. 3.17). Therefore, we consider that Palæogene sedimentary deposition during initial basin formation is neither related with the TGFS nor with the SFS and might be instead consequence of regional sag subsidence.

3.8.2 Miocene kinematics in the Tuz Gölü Basin

The distribution and cutting relationships of the different fault families found in the TGB show three deformation phases. An initial extension during Tortonian times took place after a phase of uplift and erosion [Genç and Yürür, 2010]. This local extensional phase was concentrated along the TGFS and the SFS and initiated with the onset of regional subsidence in Central Anatolia. During continued subsidence, a hitherto undocumented latest Miocene-Pliocene shortening event occurred. This shortening phase is quantitatively almost two orders of magnitude larger than the preceding and subsequent extensional phases. This relevant but relatively-short contractional period was overprinted by extension in the area, which took place during uplift of the CAP. This extension-shortening-extension succession of events is in contrast with the idea of continuous Miocene extension [Şengör and Yılmaz, 1981; Koçyiğit et al., 1995; Genç and Yürür, 2010].

3.8.3 Tectonics of the Tuz Gölü Basin

We found two different stages of basin generation, Palæogene and Late Miocene-Recent. We consider that these phases are unrelated to each other and developed as a consequence of different driving mechanisms.

The sediment geometries and faults found in the study area are in general agreement with the idea of a forearc genesis of the Palæogene basin [e.g. Görür et al., 1984]

and discard its intracratonic formation [Arıkan, 1975]. During Palæogene, crustal thickening took place in relation with the subduction of the oceanic crust of the Sakarya Continent beneath the Kışehir Massif, and a foredeep developed [e.g. Görür et al., 1984]. This mechanism is in agreement with the geometry of the Palæogene package, the relatively minor influence of the faults and the up to 2300 m of basement subsidence found in this study. However, no backthrust structures that might confirm this genetic model are found in the studied area.

The structural evidences found in the Late Miocene-Recent basin suggest that extension was acting prior to deposition of Unit 2. This extension is nearly coeval with adakitic subduction-related lavas (high Sr/Y and La/Yb ratios) in the Central Anatolia Volcanic Province [Aydar et al., 2010]. The latest Miocene shortening phase found in this study roughly coincides with the moment of surface uplift in the CAP, recently stated as younger than 8 Ma for the south of the CAP [Cosentino et al., 2012] and Late Miocene to Early Pliocene for the north of the plateau [Yıldırım et al., 2011]. Considering these simultaneous occurrences of events, we interpret that a major shortening event as young as $7 - 5$ Ma might be the cause behind the formation of the CAP.

3.9 Conclusions

The analysed seismic data indicate a complex evolution for the study area during the Miocene to Present times, in which; *(i)* a regional subsidence phase, that started in Tortonian times with the accumulation of more than 800 m of sediments, has been continuous through the Late Miocene and possibly well into Pliocene times, and *(ii)* an extensional phase, that initiated with the onset of the subsidence, was disrupted by a relevant relatively-short contractional period sometime in the latest Miocene-Pliocene, which was subsequently overprinted by extension. The fact that the vertical motions are not linked directly with the extensional/shortening events is an indication of two different types of vertical motions acting simultaneously in the area. A first order regional movement caused overall subsidence and subsequent surface uplift. Local movements of minor wavelengths appear in relation with the studied structures modulating the first order motions.